Efficient analysis of substrate integrated waveguide devices using hybrid mode matching between cylindrical and guided modes

Elena Díaz Caballero, *Graduate Student Member, IEEE,* Héctor Esteban, *Member, IEEE,* Ángel Belenguer, *Member, IEEE,* and Vicente E. Boria, *Senior Member, IEEE*

***Abstract*—A new method is presented in this paper to efficiently analyze substrate integrated waveguide (SIW) based devices with multiple accessing ports. The problem is considered as a 2-D electromagnetic problem assuming no field variation normal to the dielectric substrate. The incident and scattered fields from each circular cylinder are expanded with cylindrical modes, and the fields in the waveguide ports are expanded using progressive and regressive modal summations. The addition theorems of Bessel and Hankel functions are used to analyze the full-wave behavior of the SIW device. In order to extract the circuital parameters, the hybrid mode-matching between guided and cylindrical modes is done by projecting continuity equations in a circular boundary containing the whole SIW structure over the inner modes of each region. Applying this new technique, it is possible to analyze multiple port devices by solving a set of integrals that can be easily approached analytically or by using the inverse fast Fourier transform, avoiding the use of non efficient numerical methods. It is shown that the new method runs faster than commercial software packages and other techniques recently published.**

***Index Terms*—EM analysis, mode matching, modal analysis, substrate integrated waveguides, microwave filters.**

I. INTRODUCTION

THE interest on the substrate integrated waveguide (SIW) is constantly increasing. In such a circuit, the vertical walls of a traditional waveguide are emulated by two rows of metallic posts embedded in a dielectric substrate, which is covered with conducting sheets on the top and bottom sides. This low cost realization of the traditional waveguide circuit inherits the merits from both the microstrip for easy integration and the waveguide for low radiation loss. Furthermore, it is possible to use this new technology for making many devices, such as antennas, filters and multiplexers [1]–[3], and to integrate many substrate integrated waveguide circuits into a single-board subsystem.

E. Diaz, H. Esteban and V. E. Boria are with the Departamento de Comunicaciones, Universidad Politécnica de Valencia, 46022 Valencia, Spain (e-mail: eldiaca@iteam.upv.es; hesteban@dcom.upv.es; vboria@dcom.upv.es).

A. Belenguer is with the Departamento de Ingeniería Eléctrica, Electrónica, Automática y Comunicaciones, Escuela Universitaria Politécnica de Cuenca, Universidad de Castilla-La Mancha, Campus Universitario, 16071 Cuenca, Spain (e-mail: angel.belenguer@uclm.es).

The design equations for the radius and separation of the post walls so that the field leakage is minimum can be found in [4]–[6]. However, to study a general substrate integrated waveguide circuit, a fullwave analysis is required. For these reasons, the efficient analysis of SIW devices becomes a new challenge that is the object of intense research in the last few years.

Some of the recent contribution for the analysis of SIW circuits is based on the Boundary Integral - Resonant Mode Expansion (BI-RME) method [7]–[10], and various numerical techniques such as finite element method (FEM), finite difference time domain (FDTD), finite-difference frequency-domain (FDFD), transmission line method (TLM), and 2D multiport method have been developed to analyze the structure under consideration [11]–[14].

Other recent contributions to this field are hybrid techniques based on mode-matching and the method of moments [15] that can be used to analyze any device that is fed through canonical waveguides. In general, those hybrid techniques are formulated by applying the equivalence theorem [16], so that the ports are replaced by a pair of unknown electric and magnetic current densities. A hybrid proposal that uses this pair of currents to achieve the equivalence [17], [18] has been successfully applied to the analysis of several SIW [6], [19], [20] devices.

In [17] and also in the novel hybrid formulation recently proposed in [21], the metalized holes comprising the substrate integrated waveguide are characterized by means of cylindrical emergent spectra, implying an important computational advantage. But in [21] the port characterization is based just on a single electric current density, unlike the common strategy based on two equivalent sources, a pair of magnetic and electric current densities. This helps to reduce the computational cost, since the evaluation of the scattering parameters is much simpler, and makes possible the development of a fast sweep scheme in [22] by means of an asymptotic waveform evaluation (AWE) and the technique known as complex frequency hopping (CFH).

The aim of this work is to present a new analysis

technique in order to efficiently analyze different kinds of SIW devices with multiple accessing ports.

To achieve this objective, the multiple 2-D scattering analysis method described in [23], a method oriented toward waveguide devices that solves the matching between cylindrical and guided waves, is going to be adapted to efficiently analyze the substrate integrated waveguide devices. This method makes use of the concept of transfer function or characterization matrix of a scattering object. This matrix totally characterizes its electromagnetic behavior in the view of any incidence.

Similarly to [23], we will solve the electromagnetic coupling among all the scatterers by means of scattered cylindrical modes and spectrum translations, instead of using MoM as in [21], [22]. This procedure difference allows for an analytical resolution of the coupling, thus resulting in a method more efficient than [22], as the results section shows.

In [24] a new mode matching procedure was presented to characterize single or multiple posts inside a rectangular waveguide. This method overcomes the limitations found in [23] when the accessing ports are close to the scattering objects, but still it considers just two accesses. The circular posts were analytically characterized using cylindrical waves, and the mode matching was efficiently solved using the fast Fourier transform.

In this work, an extension of that method will allow to analyze a SIW device with multiple ports. Firstly, the whole SIW device is enclosed in a circumference as small as possible, which is not completely surrounded with accessing ports, contrary to what happened in [24]. That circular region is completely characterized through a global transfer function. Afterwards the continuity equations of electric and magnetic fields particularized in the circular boundary are projected over the cylindrical and guided modes, similarly to what is described in [24]. However, in order to solve this mode matching and to obtain the generalized scattering matrix, some of the integrals involved have had to be reformulated due to the multiple port configuration. All the integrals can still be solved analytically or by using the fast Fourier transform, thus making the new formulation highly efficient.

Finally, the results obtained in the analysis of several filters and structures are compared with different methods and commercial software, and also with experimental measurements.

II. PROBLEM FORMULATION

A. Layout of the problem

The layout of the problem, including the guided excitation accesses, the SIW device and the outer region, is presented in Fig. 1, where the three main regions are defined.

Region A includes all the guided ports accessing to the SIW device. In this region the fields will be expanded as summations of the progressive and regressive guided modes. Region B is a circular region containing the whole SIW device. In this inner region, the fields will be expressed as summations of incident and scattered cylindrical open space modes. Finally, region C is the outer region, in which the fields should be zero since the leakage form the post walls is very weak. The analysis of each region and the mode matching is presented below.

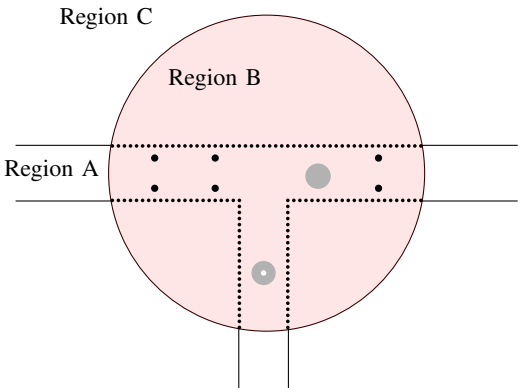

Fig. 1: Layout of a general SIW problem

B. Scattering objects

Region B, containing the SIW device, can be seen as a multiple scattering problem with N scattering objects. Every single object receives incident fields from the external excitation but also scattered fields coming from the other N-1 objects. It will be necessary to solve the electromagnetic coupling among scatterers. This multiple scattering problem can be schematized as shown in Fig. 2.

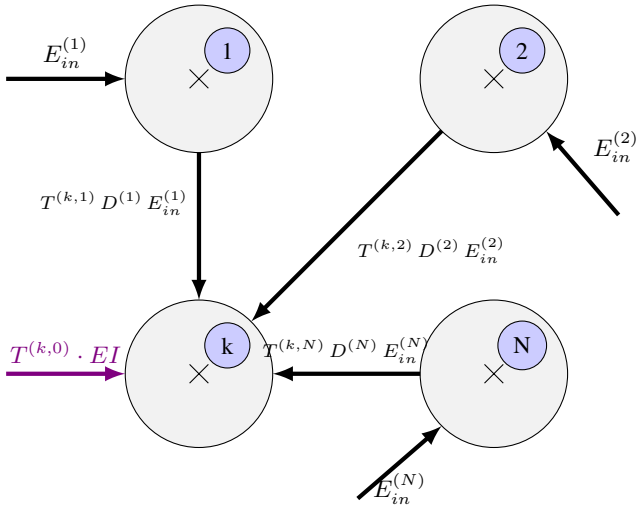

Fig. 2: Multiple scattering scheme with incident fields to object k

Since the geometry of the scattering objects is invariant in z, and so are the exciting fields, the scattered fields are

also invariant in z and the structure can be reduced to a 2-D problem, where a cylindrical coordinate system will be used. For each scattering object, the field is expanded as summations of incident and scattered cylindrical modes as follows

$$\vec{E}_i^{(k)} = \sum_{p=-N_i^{(k)}}^{N_i^{(k)}} i_p^{(k)}\, J_p(k\rho^{(k)})\, e^{jp\phi^{(k)}}\, \hat{z} \qquad (1)$$

$$\vec{E}_d^{(k)} = \sum_{q=-N_d^{(k)}}^{N_d^{(k)}} c_q^{(k)}\, H_q^{(2)}(k\rho^{(k)})\, e^{jq\phi^{(k)}}\, \hat{z} \qquad (2)$$

where $i_p^{(k)}$ and $c_q^{(k)}$ are the incident and scattered field spectra in open space to object k, $J_p(k\rho^{(k)})\, e^{jp\phi^{(k)}}$ and $H_q^{(2)}(k\rho^{(k)})\, e^{jq\phi^{(k)}}$ are the p-th incident and q-th scattered cylindrical modes, and $N_i^{(k)}$ and $N_d^{(k)}$ are the truncation indexes for the summations of incident and scattered cylindrical modes. Both numbers must be high enough to ensure a good accuracy of the results [16], [25], [26]. In this work, considering the general case of $K = \omega\sqrt{\mu\varepsilon}$, where $\varepsilon = \varepsilon'(1 - j\tan\delta)$ and $\tan\delta$ represents the loss tangent in the dielectric substrate, the following expression has been used

$$N_i^{(k)} = \max\left\{3,\ \text{ceil}\left(PNi^{(k)} \cdot \Re(K) r^{(k)}\right)\right\} \qquad (3)$$

$$N_d^{(k)} = \max\left\{3,\ \text{ceil}\left(PNd^{(k)} \cdot \Re(K) r^{(k)}\right)\right\} \qquad (4)$$

where $\Re(K)$ is the real part of the wavenumber, K, $r^{(k)}$ is the radius of object k and $PNi^{(k)}$ and $PNd^{(k)}$ are values high enough to guarantee good accuracy inside the validity region of the modal expansion, though it is advisable not to over estimate those truncation indexes as it leads to an unnecessary increase in the computational cost of the analysis method. With these equations, we ensure that $N_i^{(k)}$ and $N_d^{(k)}$ are at least 3, in order to avoid a excessively low number of modes if object k has a very small radius. In (1) and (2), $\rho^{(k)}$ and $\phi^{(k)}$ are the polar coordinates in the coordinate system local to object k (see Fig. 3). It is convenient to place the local coordinate system of the object k so that the larger distance from it to any point of the object, $r^{(k)}$, is minimum. As the typical scatterer will be a cylindrical object, $r^{(k)} = a^{(k)}$ where $a^{(k)}$ is the radius of the cylinder. A convergence study will be presented in Section II-F.

In region B, the field spectrum scattered by each object can be related to its incident field spectrum by means of the scattering matrix $D^{(k)}$, which provides the full wave characterization of that scattering object k [25] as follows

$$c_q^{(k)} = \sum_{p=-N_i^{(k)}}^{N_i^{(k)}} i_p^{(k)}\, d_{qp}^{(k)} \qquad (5)$$

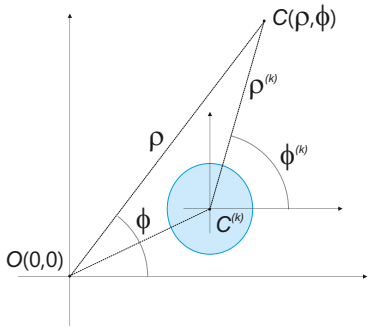

Fig. 3: Coordinate system local to object k and global coordinate system

In matrix form

$$ED^{(k)} = D^{(k)} \cdot EI^{(i)} \qquad (6)$$

where $ED^{(k)}$ and $EI^{(i)}$ are, respectively, scattered and incident field spectra for object k.

In this work, we have considered different types of scattering objects, whose scattering matrices [16] [27] have been adapted from the vacuum assumption to the the case in which the objects are immersed in a dielectric substrate. Their scattering matrices are presented below.

When the scattering object k is a circular post, each incident cylindrical mode excites only the scattered cylindrical mode of the same order, so truncation indexes $N_i^{(k)}$ and $N_d^{(k)}$ in (3) and (4) must be the same. Thus the scattering matrix that relates incident and scattered cylindrical spectra is a diagonal matrix [16], and

$$d_{qp}^{(k)} = 0, \qquad \forall q \neq n \qquad (7)$$

$$c_q^{(k)} = \sum_{p=-N_i^{(k)}}^{N_i^{(k)}} d_{qp}^{(k)}\, i_p^{(k)} = d_{qq}^{(k)}\, i_q^{(k)} \qquad (8)$$

The most common scattering object presented in a SIW device is the metallic cylinder, whose scattering matrix elements can be easily obtained analytically [16],

$$d_{qq}^{(k)} = -\frac{J_q(Ka^{(k)})}{H_q^{(2)}(Ka^{(k)})} \qquad (9)$$

where $a^{(k)}$ is the radius of cylinder k and $K = \frac{\omega}{c_0}\sqrt{\mu_r\varepsilon_r}$ is the substrate wavenumber, being $\varepsilon_r = \varepsilon_r^{'} - j\varepsilon_r^{''} = \varepsilon_r^{'}(1 - j\tan\delta)$ and μ_r the relative permittivity and permeability of the dielectric substrate. The dielectric and the multilayer cylinder have been also considered.

The scattering matrix of a dielectric post,

$$d_{qq}^{(k)} = \frac{\begin{vmatrix} J_q(Ka^{(k)}) & J_q(K_c a^{(k)}) \\ J_q'(Ka^{(k)}) & J_q'(K_c a^{(k)}) \sqrt{\frac{\varepsilon_{r_c}^{(k)}/\varepsilon_r}{\mu_{r_c}^{(k)}/\mu_r}} \end{vmatrix}}{\begin{vmatrix} -H_q^{(2)}(Ka^{(k)}) & J_q(K_c a^{(k)}) \\ -H_q^{'(2)}(Ka^{(k)}) & J_q'(K_c a^{(k)}) \sqrt{\frac{\varepsilon_{r_c}/\varepsilon_r}{\mu_{r_c}/\mu_r}} \end{vmatrix}} \qquad (10)$$

will be useful not only to characterize a real dielectric post, but also for a metallic post with losses, where the relative permittivity of the post with finite conductivity is

$$\varepsilon_{r_c} = -j\frac{\sigma}{\varepsilon_0 \omega}$$

σ is the finite conductivity of the metal and $K_c = \frac{\omega}{c_0}\sqrt{\varepsilon_{r_c}}\sqrt{\mu_{r_c}}$ is the wavenumber inside the cylinder.

In the case of a multilayer cylinder, the iterative method to solve its scattering matrix is introduced in [27], though the last layer, generally assumed to be vacuum, will have here $\varepsilon_r > 1$ because of the dielectric substrate.

C. Electromagnetic coupling among scatterers

In order to solve the electromagnetic coupling, the general method introduced in [25] is adapted to efficiently solve the particular situation faced in a SIW structure. This method will allow us to forget about the geometry of each scattering object once its scattering matrix is known.

As shown in Fig. 2, matrix $T^{(k,i)}$ is a spectrum translation matrix from cylindrical spectrum emergent from $C^{(i)}$ to cylindrical spectrum incident to $C^{(k)}$, whose elements are

$$T_{pq}^{(k,i)} = H_{p-q}^{(2)}(Kd^{(k,i)})\, e^{-j(p-q)\phi^{(i,k)}} \tag{11}$$

where

$$d^{(k,i)} = \sqrt{(x_{C^{(i)}} - x_{C^{(k)}})^2 + (y_{C^{(i)}} - y_{C^{(k)}})^2} \tag{12}$$

$$\tan\phi^{(k,i)} = \frac{y_{C^{(i)}} - y_{C^{(k)}}}{x_{C^{(i)}} - x_{C^{(k)}}} \tag{13}$$

and $T^{(k,0)}$ is the translation matrix from external spectrum incident to O, where O is the global coordinate origin (see Fig. 5), to cylindrical spectrum incident to $C^{(k)}$, whose elements are

$$T_{rp}^{(k,0)} = J_{r-p}(Kd^{(k,0)})\, e^{-j(r-p)\phi^{(k,0)}} \tag{14}$$

The final equation system for the field incident to object k can be written as follows (see Fig. 2)

$$E_{in}^{(k)} = T^{(k,0)} \cdot EI + \sum_{i=1, i\neq k}^{N} T^{(k,i)} \cdot D^{(i)} \cdot E_{in}^{(i)}$$

$$\sum_{k=1}^{N} A^{(k,i)} \cdot E_{in}^{(i)} = T^{(k,0)} \cdot EI \qquad k = 1, \ldots, N \tag{15}$$

$$A^{(k,i)} = \begin{cases} I & \text{si } k = i \\ -T^{(k,i)} \cdot D^{(i)} & \text{si } k \neq i \end{cases} \tag{16}$$

where I is an $(2N_i^{(k)}+1)\times(2N_i^{(k)}+1)$ identity matrix and EI is the incident external field spectrum characterized with $2N_i + 1$ cylindrical modes, where

$$N_i = \text{ceil}(PNi \cdot \Re K \cdot R) \tag{17}$$

and R is the radius of the circular boundary (see Fig. 5).

Finally, the matrix system to be solved for the electromagnetic coupling among N scattering objects is

$$E = A^{(-1)} \cdot B \cdot EI \tag{18}$$

where

$$E = [E_{in}^{(1)}, \ldots E_{in}^{(N)}]^T \qquad B = [T^{(1,0)}, \ldots T^{(N,0)}]^T \tag{19}$$

It will be useful to define the coupled scattering matrix of the object k, $D^{'(k)}$, as the one that completely characterizes object k taking into account the coupling with all the other objects. In order to do so, the external excitation matrix EI in (18) is supposed to be an identity matrix, having

$$E^{'} = A^{(-1)} \cdot B$$

where $E^{'}$ contains N submatrices $E^{'(k)}$. Each submatrix stores the total incident field to object k for each external incident mode. The product of $E^{'(k)}$ and $D^{(k)}$ results in the wanted $D^{'(k)}$

$$D^{'(k)} = D^{(k)} \cdot E^{'(k)}$$

In Fig. 4 the amplitude of the total electric field obtained in this way is represented for a four cavity SIW filter with an incident plane wave, whose cylindrical spectrum is [16]

$$i_n = (je^{j\beta_0})^{-n}$$

where $\phi = \beta_0$ is the propagation direction, here taken as $\beta_0 = 0$rad.

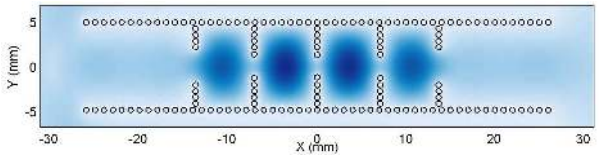

Fig. 4: Electric field amplitude with an 11GHz incident plane wave propagating parallel to the x axis

D. Global Scattering Matrix

Before obtaining a circuital matrix that characterizes the SIW device, a global scattering matrix is needed. In order to do so, the whole SIW structure must be contained in a circumference as small as possible. This is to obtain the D_{global} scattering matrix of the whole SIW part of the problem, relating the scattered field spectrum to the incident one.

The global scattering matrix comes from adding all the contributions of the scattered fields of every single post, but centered in the center of the circumference containing all of them (see Fig. 5), which will be also the center

of the global coordinate system. It can be calculated as follows,

$$D_{global} = \sum_{k=1}^{N} T^{(0,k)}\, D^{'(k)} \quad N \equiv \text{number of posts} \tag{20}$$

where $D^{'(k)}$ is the coupled scattering matrix of the k-object and $T^{(0,k)}$ is the translation matrix from $C^{(k)}$ to O

$$T_{rp}^{(0,k)} = J_{r-p}(Kd^{(0,k)})\, e^{-j(r-p)\phi^{(0,k)}} \tag{21}$$

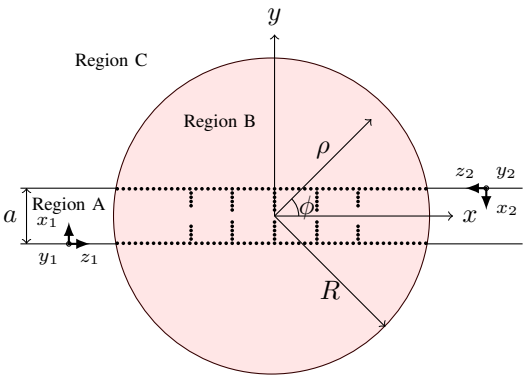

Fig. 5: General layout of the SIW problem with coordinate systems of regions A and B

This matrix will not be a diagonal one, but it is convenient to make it square by filling it with zeros. Although D_{global} has all the information concerning the electromagnetic behavior of the SIW structure, it is necessary to express that information in terms of circuit parameters in order to link it to other blocks using simple circuit theory.

E. Generalized Scattering Matrix. Mode Matching

Now, in order to obtain the circuital parameters of the SIW device, a mode matching between guided modes of Region A and cylindrical modes of Region B must be done. This can be achieved by enforcing continuity of tangential components of electric and magnetic fields in the circumference of radius R containing Region B. This leads to the Generalized Scattering Matrix (GSM).

In **region B**, the field can be expanded as summations of incident and scattered cylindrical modes,

$$\vec{E} = \vec{E}^{in}(\rho,\phi) + \vec{E}^{d}(\rho,\phi) \tag{22}$$

$$\vec{E}^{in}(\rho,\phi) \approx \sum_{p=-N_i}^{N_i} i_p\, J_p(k\rho)\, e^{jp\phi}\, \hat{z} \tag{23}$$

$$\vec{E}^{d}(\rho,\phi) \approx \sum_{p=-N_i}^{N_i} \sum_{n=-N_d}^{N_d} d_{np}\, i_p\, H_n^{(2)}(k\rho)\, e^{jn\phi}\, \hat{z} \tag{24}$$

where N_i (17) and N_d are the truncation indexes for the summations,

$$N_d = \text{ceil}(PNd \cdot K \cdot R) \tag{25}$$

(where, according to [16], $PNd \geq 1$) and d_{np} are the elements of the D_{global} matrix.

In **region A**, the tangential fields are expanded as summations of the progressive and regressive guided modes of the canonical equivalent waveguide, whose width, a_{eq}, can be calculated as [28]

$$\frac{a_{eq}}{w} = \xi_1 + \frac{\xi_2}{\frac{s}{d} + \frac{\xi_1+\xi_2-\xi_3}{\xi_3-\xi_1}} \tag{26}$$

$$\xi_1 = 1.0198 + \frac{0.3465}{\frac{w}{s} - 1.0684}$$

$$\xi_2 = -0.1183 - \frac{1.2729}{\frac{w}{s} - 1.2010}$$

$$\xi_3 = 1.0082 - \frac{0.9163}{\frac{w}{s} + 0.2152}$$

where w is the distance between the two rows of metallic vias comprising the SIW walls, s is repetition period or separation between the center of consecutive vias, and d is their diameter.

The expressions for the fields are [21], [25]

$$\vec{E}_t^{(i)}(\rho,\phi) = \sum_{m=1}^{M_i} (a_m^{(i)}\, e^{-\gamma_m^{(i)} z_i} + b_m^{(i)}\, e^{\gamma_m^{(i)} z_i})\vec{e}_m^{(i)''}(x_i) \tag{27}$$

$$\vec{H}_t^{(i)}(\rho,\phi) = \sum_{m=1}^{M_i} (a_m^{(i)}\, e^{-\gamma_m^{(i)} z_i} - b_m^{(i)}\, e^{\gamma_m^{(i)} z_i})\, Y_{0m}^{(i)} \vec{h}_m^{(i)''}(x_i) \tag{28}$$

$$\gamma_m^{(i)} = \sqrt{\left(\frac{m\pi}{a_{eq}^{(i)}}\right)^2 - k^2} \tag{29}$$

$$Y_{m0}^{(i)} = \frac{1}{Z_{m0}^{(i)}} = \frac{\gamma_m^{(i)}}{j\omega\mu} = \frac{\gamma_m^{(i)}}{jk\eta} \tag{30}$$

where $a_m^{(i)}$ y $b_m^{(i)}$ are the amplitudes of the progressive and regressive TE_{m0} guided modes at access i, M_i is the number of modes in that access, and $i = 1, ..., L$, being L the total number of accessing ports,

$$\vec{e}_m^{(i)''}(x_i) = \begin{cases} -\hat{z}\sqrt{\frac{2\, Z_{0m}^{(i)}}{a_{eq}^{(i)} h}}\, \sin\left(\frac{m\pi}{a_{eq}^{(i)}} x_i\right) & \phi \in [\phi_m^{(i)}, \phi_M^{(i)}] \\ 0 & \text{other} \end{cases} \tag{31}$$

$$\vec{h}_m^{(i)''}(x_i) = \begin{cases} \hat{x}_i\sqrt{\frac{2\, Z_{0m}^{(i)}}{a_{eq}^{(i)} h}}\, \sin\left(\frac{m\pi}{a_{eq}^{(i)}} x_i\right) & \phi \in [\phi_m^{(i)}, \phi_M^{(i)}] \\ 0 & \text{other} \end{cases} \tag{32}$$

with h being the substrate height, and $\phi_m^{(i)}$ and $\phi_M^{(i)}$ are the ϕ coordinates in the global coordinate system of the port i edges (see Fig. 6).

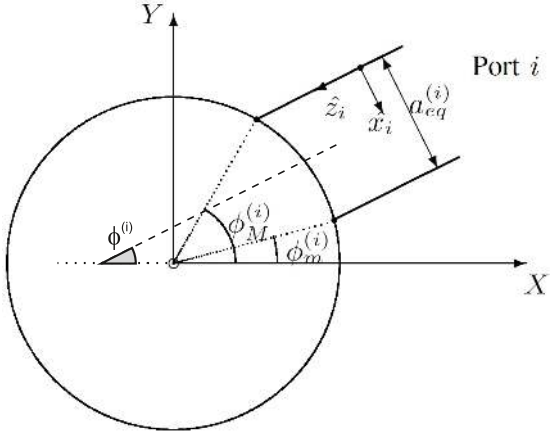

Fig. 6: Local to port i and global coordinate systems

In a more compact way, and considering $\rho = R$, (27) and (28) can be written in terms of global cylindrical coordinate system as

$$\vec{E}_t(\phi) = \sum_{m=1}^{M} \left(a_m\, e_m^{+}(\phi) + b_m\, e_m^{-}(\phi)\right)\, g_m\,(\phi)\,(-\hat{z}) \quad (33)$$

$$\vec{H}_t(\phi) = \sum_{m=1}^{M} \left(a_m\, e_m^{+}(\phi) - b_m\, e_m^{-}(\phi)\right)\, Y_{0m}\, g_m\,(\phi)\,\hat{x}_i \quad (34)$$

defining vectors a, b and Y_0, each of them with $M = \sum_{i=1}^{L} M_i$ elements,

$$a = \begin{bmatrix} a^{(1)} \\ a^{(2)} \\ \vdots \\ a^{(L)} \end{bmatrix} \quad b = \begin{bmatrix} b^{(1)} \\ b^{(2)} \\ \vdots \\ b^{(L)} \end{bmatrix} \quad Y_0 = \begin{bmatrix} Y_0^{(1)} \\ Y_0^{(2)} \\ \vdots \\ Y_0^{(L)} \end{bmatrix} \quad (35)$$

where

$$a^{(i)} = \left[a_1^{(i)}, ..., a_{M_i}^{(i)}\right]^T, i \in [1, ..., L] \quad (36)$$

$$b^{(i)} = \left[b_1^{(i)}, ..., b_{M_i}^{(i)}\right]^T, i \in [1, ..., L] \quad (37)$$

$$Y_0^{(i)} = \left[Y_{01}^{(i)}, ..., Y_{0M_i}^{(i)}\right]^T, i \in [1, ..., L] \quad (38)$$

and defining also the vectors in (39) and (40), where $\phi_0^{(i)}$ is the coordinate ϕ just in the angular center of access i (see Fig. 6)

$$\phi_0^{(i)} = \frac{\phi_m^{(i)} + \phi_M^{(i)}}{2}$$

and $\phi_d^{(i)}$ is the angular width of that access ($\phi_d^{(i)} = \phi_M^{(i)} - \phi_m^{(i)}$).

Since the post walls are designed to emulate the vertical walls of the traditional waveguide circuit using the design rules in [4] and [6], the field leakage from the post walls is very weak, and thus the field in **region C** can be neglected. Note that if a little leakage occurred, it would be still in region B and would be vanished by the time it arrives to the border with region C.

Next, continuity of tangential components is going to be enforced. Eqs. (33) and (34) of region A are already particularized in the circumference of radius R. In region B, the transversal electric field particularized in the circular boundary is

$$\vec{E}_i(\rho = R) + \vec{E}_d(\rho = R) = \sum_{n=-N_i}^{N_i} (J_n(KR)e^{jn\phi} + \sum_{q=-N_d}^{N_d} d_{qn} H_q^{(2)}(KR)e^{jq\phi}) i_n \hat{z} \quad (41)$$

Enforcing tangential field continuity in the circumference of radius R, electric fields in (33) and (41) must be equal in $\rho = R$.

$$\vec{E}_i(\rho = R, \phi) + \vec{E}_d(\rho = R, \phi) = \vec{E}_t(\rho = R, \phi) \quad (42)$$

Using Maxwell's curl equation, $\vec{H} = -\frac{1}{j\omega\mu}\nabla \times \vec{E}$, we can also obtain the total magnetic field in the inner region

$$\vec{H}(\rho = R) = \sum_{n=-N_i}^{N_i} [-\frac{1}{\eta}\frac{n}{KR}(J_n(KR)e^{jn\phi} + \sum_{q=-N_d}^{N_d} q\, d_{qn} H_q^{(2)}(KR)e^{jq\phi})\hat{\rho} - \frac{1}{\eta}(J_n^{'}(KR)e^{jn\phi} + \sum_{q=-N_d}^{N_d} d_{qn} H_q^{(2)'}(KR)e^{jq\phi})\hat{\phi}] i_n \quad (43)$$

where η is the intrinsic impedance of the substrate ($\eta = 120\pi/\sqrt{\varepsilon_r}$). The continuity equation of magnetic field along $\hat{t} = \hat{x}_i$ results as follows

$$[\vec{H}^{in}(\rho = R, \phi) + \vec{H}^{sc}(\rho = R, \phi)] \cdot \hat{t} = \sum_{i=1}^{N} \left[\vec{H}_t^{(i)}(\rho = R, \phi) \cdot \hat{t} + \vec{H}_{z_i}^{(i)}(\rho = R, \phi) \cdot \hat{t}\right] = \sum_{i=1}^{N} \vec{H}_t^{(i)}(\rho = R, \phi) \cdot \hat{x}_i \quad (44)$$

where

$$[\vec{H}_t^{in}(R, \phi) + \vec{H}_t^{sc}(R, \phi)] \cdot \hat{t} = \sum_{n=-N_i}^{N_i} [-\frac{1}{\eta}\frac{n}{KR}(J_n(KR)e^{jn\phi} + \sum_{q=-N_d}^{N_d} q\, d_{qn} H_q^{(2)}(KR)e^{jq\phi})(\hat{\rho} \cdot \hat{t}) - \frac{1}{\eta}(J_n^{'}(KR)e^{jn\phi} + \sum_{q=-N_d}^{N_d} d_{qn} H_q^{(2)'}(KR)e^{jq\phi})(\hat{\phi} \cdot \hat{t})] i_n \quad (45)$$

$$e_m^{\pm}(\phi) = \begin{cases} e^{\mp\gamma_m^{(1)} z_1(R,\phi)} \cdot \prod \left(\frac{\phi - \phi_0^{(1)}}{\phi_d^{(1)}} \right) & \text{si } m \in [1, ..., M_1] \\ e^{\mp\gamma_{m-M_1}^{(2)} z_2(R,\phi)} \cdot \prod \left(\frac{\phi - \phi_0^{(2)}}{\phi_d^{(2)}} \right) & \text{si } m \in [M_1+1, ..., M_1+M_2] \\ \vdots & \\ e^{\mp\gamma_{m-\sum_{j=1}^{L-1} M_j}^{(N)} z_N(R,\phi)} \cdot \prod \left(\frac{\phi - \phi_0^{(N)}}{\phi_d^{(N)}} \right) & \text{si } m \in \left[\sum_{j=1}^{N-1} M_j + 1, ..., M \right] \\ 0 & \text{other} \end{cases} \quad (39)$$

$$g_m(\phi) = \begin{cases} h_m^{(1)''}(x_1(R,\phi)) \cdot \prod \left(\frac{\phi - \phi_0^{(1)}}{\phi_d^{(1)}} \right) & \text{si } m \in [1, ..., M_1] \\ h_{m-M_1}^{(2)''}(x_2(R,\phi)) \cdot \prod \left(\frac{\phi - \phi_0^{(2)}}{\phi_d^{(2)}} \right) & \text{si } m \in [M_1+1, ..., M_1+M_2] \\ \vdots & \\ h_{m-\sum_{j=1}^{N-1} M_j}^{(N)''}(x_N(R,\phi)) \cdot \prod \left(\frac{\phi - \phi_0^{(N)}}{\phi_d^{(N)}} \right) & \text{si } m \in \left[\sum_{j=1}^{L-1} M_j + 1, ..., M \right] \\ 0 & \text{other} \end{cases} \quad (40)$$

and

$$\hat{t} = \hat{x}_i = \sin\phi^{(i)}\hat{x} - \cos\phi^{(i)}\hat{y} \quad (46)$$

$$\hat{\rho} = \cos\phi\,\hat{x} + \sin\phi\,\hat{y} \quad (47)$$

$$\hat{\phi} = -\sin\phi\hat{x} + \cos\phi\hat{y} \quad (48)$$

$$\hat{\rho}\cdot\hat{x}_i = A^{(i)}\cos\phi + B^{(i)}\sin\phi \quad (49)$$

$$\hat{\phi}\cdot\hat{x}_i = B^{(i)}\cos\phi - A^{(i)}\sin\phi \quad (50)$$

$$A = \begin{bmatrix} \sin\phi^{(1)} \\ \sin\phi^{(2)} \\ \vdots \\ \sin\phi^{(L)} \end{bmatrix} \quad (51)$$

$$B = \begin{bmatrix} -\cos\phi^{(1)} \\ -\cos\phi^{(2)} \\ \vdots \\ -\cos\phi^{(L)} \end{bmatrix} \quad (52)$$

$A^{(i)}$ and $B^{(i)}$ are, respectively, the components in $\hat{x}$ and $\hat{y}$ of vector $\hat{x}_i$ in each of the L accesses. However, A_{mn} and B_{mn} will be used instead

$$A_{mn} = \begin{cases} \sin\phi^{(1)} & m \in [1, ..., M_1] & n \in [-N_i, N_i] \\ \sin\phi^{(2)} & m \in [M_1+1, ..., M_1+M_2] & n \in [-N_i, N_i] \\ \vdots & & \\ \sin\phi^{(L)} & m \in [\sum_{i=1}^{L-1} M_i + 1, ..., M] & n \in [-N_i, N_i] \end{cases} \quad (53)$$

$$B_{mn} = \begin{cases} -\cos\phi^{(1)} & m \in [1, ..., M_1] & n \in [-N_i, N_i] \\ -\cos\phi^{(2)} & m \in [M_1+1, ..., M_1+M_2] & n \in [-N_i, N_i] \\ \vdots & & \\ -\cos\phi^{(L)} & m \in [\sum_{i=1}^{L-1} M_i + 1, ..., M] & n \in [-N_i, N_i] \end{cases} \quad (54)$$

where $\phi^{(i)}$ is the angle that the excitation line accessing to port-i forms with axis X in the global coordinate system, that is $(\widehat{\hat{x}, \hat{z}_i})$ (see Fig. 6).

Instead of using discrete mode matching, and due to the circular boundary, in this work the mode matching is solved by projecting the equations resulting from enforcing field continuity to the modes of A and B. This provides with a set of equations, and after selecting the proper ones, a matrix system is obtained whose solution is the GSM of the structure. If the right set of equations is chosen [24], the matrix system will be really well conditioned and achieve a good accuracy in the results. Moreover, the integrals that must be solved to obtain the elements of the matrices involved can be solved by using the fast Fourier transform instead of using other numerical methods.

In order to obtain an equation system, (42) and (44) must be projected over the modes of the regions A or B. Projecting (42) over the inner modes of region B, $e^{jm\phi}$, gives

$$\sum_{n=-N_i}^{N_i} I_{mn} i_n = \sum_{n=1}^{M} (J_{mn} a_n + K_{mn} b_n) \quad (55)$$

where $m \in [-N_i, N_i]$ and

$$I_{mn} = \int_0^{2\pi} E_t^B(\rho = R) \cdot e^{-jm\phi} d\phi \quad (56)$$

$$J_{mn} = \int_0^{2\pi} e_n^+(\phi) g_n(\phi) e^{-jm\phi} d\phi \quad (57)$$

$$K_{mn} = \int_0^{2\pi} e_n^-(\phi) g_n(\phi) e^{-jm\phi} d\phi \quad (58)$$

(59)

Projecting (44) over the modes of the region A, $g_m(\phi)$ gives

$$\sum_{n=-N_i}^{N_i} R_{mn} i_n = \sum_{n=1}^{M} (U_{mn} a_n - T_{mn} b_n) \quad (60)$$

where $m \in [0, M]$,

$$R_{mn} = \int_0^{2\pi} H_t^B(\rho = R) \cdot g_m^*(\phi) d\phi \quad (61)$$

$$U_{mn} = \int_0^{2\pi} e_n^+(\phi) Y_{0n} g_n(\phi) g_m^*(\phi) d\phi \quad (62)$$

$$T_{mn} = \int_0^{2\pi} e_n^-(\phi) Y_{0n} g_n(\phi) g_m^*(\phi) d\phi \quad (63)$$

Expressing equations (55) and (60) in matrix form

$$Ii = Ja + Kb \quad (64)$$

$$Ri = Ua - Tb \quad (65)$$

In order to obtain the GSM, (64) and (65) contain information of both electric and magnetic fields. i will be extracted from (64)

$$i = I^{-1}(Ja + Kb) \quad (66)$$

Now substituting in (66) in (65)

$$RI^{-1}(Ja + Kb) = Ua - Tb \quad (67)$$

$$(U - RI^{-1}J)a = (T + RI^{-1}K)b \quad (68)$$

And finally, the GSM is $(b = Sa)$

$$\boxed{S = (T + RI^{-1}K)^{-1}(U - RI^{-1}J)} \quad (69)$$

With this procedure, we have used the equation (64) of the electric field continuity projected over the modes of region B, and the equation (65) of the magnetic field continuity projected over the modes of region A. So both electric and magnetic fields have been used and projections over both sets of modes, those of region A and those of region B, are involved.

The great advantage of this analysis method is that all the integrals needed for the elements of matrices I, J, K, R, T and U can be solved either analytically or by using the fast Fourier transform. It is in the evaluation of R where a new reformulation has been required in order to adapt the mode matching presented in [24] to the case or multiple accesses (see [24] for expressions of the other five types of integrals).

R_{mn} (eq. 61) comes from the projection of transversal magnetic fields of the inner region over the guided modes

$$\begin{aligned} R_{mn} = & \int_0^{2\pi} -\frac{1}{\eta}\frac{n}{KR} J_n(KR) e^{jn\phi} \left[A_{mn} \left(\frac{e^{j\phi} + e^{-j\phi}}{2} \right) + \right. \\ & + B_{mn} \left(\frac{e^{j\phi} - e^{-j\phi}}{2j} \right) g_m^*(\phi) d\phi + \\ & + \int_0^{2\pi} -\frac{1}{\eta}\frac{q}{KR} \sum_q d_{qn} H_q^{(2)}(KR) e^{jq\phi} \left[A_{mn} \left(\frac{e^{j\phi} + e^{-j\phi}}{2} \right) + \right. \\ & + B_{mn} \left(\frac{e^{j\phi} - e^{-j\phi}}{2j} \right) g_m^*(\phi) d\phi + \\ & + \int_0^{2\pi} -\frac{j}{\eta} J_n'(KR) e^{jn\phi} \left[B_{mn} \left(\frac{e^{j\phi} + e^{-j\phi}}{2} \right) - \right. \\ & - A_{mn} \left(\frac{e^{j\phi} - e^{-j\phi}}{2j} \right) g_m^*(\phi) d\phi + \\ & + \int_0^{2\pi} -\frac{j}{\eta} \sum_q d_{qn} H_q^{(2)'}(KR) e^{jq\phi} \left[B_{mn} \left(\frac{e^{j\phi} + e^{-j\phi}}{2} \right) - \right. \\ & \left. - A_{mn} \left(\frac{e^{j\phi} - e^{-j\phi}}{2j} \right) g_m^*(\phi) d\phi \right. \end{aligned} \quad (70)$$

Using (81) and substituting in (70),

$$\begin{aligned} R_{mn} \cong & -\frac{\pi}{\eta}\frac{n}{KR} J_n(KR) \left[(A_{mn} - jB_{mn}) \tilde{y}^{(m)}[n+1] + \right. \\ & + (A_{mn} + jB_{mn}) \tilde{y}^{(m)}[n-1] + \\ & - \frac{\pi}{\eta}\frac{q}{KR} \sum_q d_{qn} H_q^{(2)}(KR) \left[(A_{mn} - jB_{mn}) \tilde{y}^{(m)}[q+1] + \right. \\ & + (A_{mn} + jB_{mn}) \tilde{y}^{(m)}[q-1] + \\ & - \frac{j\pi}{\eta} J_n'(KR) \left[(B_{mn} + jA_{mn}) \tilde{y}^{(m)}[n+1] + \right. \\ & + (B_{mn} - jA_{mn}) \tilde{y}^{(m)}[n-1] + \\ & - \frac{j\pi}{\eta} \sum_q d_{qn} H_q^{(2)'}(KR) \left[(B_{mn} + jA_{mn}) \tilde{y}^{(m)}[q+1] + \right. \\ & \left. + (B_{mn} - jA_{mn}) \tilde{y}^{(m)}[q-1] \right. \end{aligned} \quad (71)$$

In matrix form

$$R = \pi Y^+ (R^A + R^B D) + \pi Y^- (R^C + R^D D) \quad (72)$$

where

$$Y^+ = \begin{bmatrix} \tilde{y}^{(1)}[n+1] \\ \tilde{y}^{(2)}[n+1] \\ \vdots \\ \tilde{y}^{(M)}[n+1] \end{bmatrix}_{M \times (2N_i+1)} \quad (73)$$

$$Y^- = \begin{bmatrix} \tilde{y}^{(1)}[n-1] \\ \tilde{y}^{(2)}[n-1] \\ \vdots \\ \tilde{y}^{(M)}[n-1] \end{bmatrix}_{M \times (2N_i+1)} \quad (74)$$

and R^A, R_B, R_C and R_D are diagonal matrices with

$$\begin{aligned} R^A_{nn} &= -\frac{1}{\eta}\frac{n}{KR}J_n(KR)\,(A_{mn}-jB_{mn}) \\ &\quad -j\frac{1}{\eta}J_n^{'}(KR)\,(B_{mn}+jA_{mn}) \qquad (75) \\ R^B_{nn} &= -\frac{1}{\eta}\frac{q}{KR}H_q^{(2)}(KR)\,(A_{mn}-jB_{mn}) \\ &\quad -j\frac{1}{\eta}H_q^{(2)'}(KR)\,(B_{mn}+jA_{mn}) \qquad (76) \\ R^C_{nn} &= -\frac{1}{\eta}\frac{n}{KR}J_n(KR)\,(A_{mn}+jB_{mn}) \\ &\quad -j\frac{1}{\eta}J_n^{'}(KR)\,(B_{mn}-jA_{mn}) \qquad (77) \\ R^D_{nn} &= -\frac{1}{\eta}\frac{q}{KR}H_q^{(2)}(KR)\,(A_{mn}+jB_{mn}) \\ &\quad -j\frac{1}{\eta}H_q^{(2)'}(KR)\,(B_{mn}-jA_{mn}) \qquad (78) \end{aligned}$$

Finally,

$$\begin{aligned} R = \pi Y^+(A_{mn}+jB_{mn})(R^a+R^bD)+ \\ +\pi Y^-(A_{mn}-jB_{mn})(R^c+R^dD) \end{aligned}$$

where

$$y^{(m)}[n] = DTFT^{-1}\{g_m^*(\phi)\} \qquad (80)$$

but in order to accelerate the process, just some discrete points of $g_m^*(\phi)$ are considered along ϕ and Fast Fourier Transform can be used,

$$y^{(m)}[n] \approx \tilde{y}^{(m)}[n] = FFT^{-1}\{g_m^*(\phi)\} \qquad (81)$$

being $\tilde{y}^{(m)}[n]$ a periodic signal with period equal to the number of discrete points considered for the FFT. This number of points must be

$$N_{fft} \geq 2N_i + 1$$

so that aliasing error will not appear, and the following expression has been used

$$N_{fft} = 2 \cdot \text{ceil}(N_i(1+PN_{fft})) + 1 \qquad (82)$$

Properties of FFT that have been utilized are

$$\frac{1}{2\pi}\int_0^{2\pi} g_m^*(\phi)e^{j\phi}e^{jn\phi}d\phi = y^{(m)}[n+1] \cong \tilde{y}^{(m)}[n+1] \qquad (83)$$

$$\frac{1}{2\pi}\int_0^{2\pi} g_m^*(\phi)e^{-j\phi}e^{jn\phi}d\phi = y^{(m)}[n-1] \cong \tilde{y}^{(m)}[n-1] \qquad (84)$$

F. Convergence study

Due to computational reasons, several infinite summations must be truncated. Truncation indexes for the number of modes of the external incident field spectrum, N_i (17), the scattered field spectrum, N_d (25), and the incident field spectrum to object k, $N_i^{(k)}$ (3), and for the number of points of the FFT, N_{fft} (82), have been defined.

In order to test the convergence of the method and choose the adequate values for these indexes, a similar convergence study as in [24] has been done with each one of these indexes. It shows that the adequate values in this new formulation of hybrid mode matching are $PN_i^{(k)} = 7$, $PNi = 10$, $PNd = 1.5$ and $PN_{fft} = 2$. This is to ensure that the chosen parameters are valid for a wide range of different complex structures.

III. RESULTS

We have tested the efficiency and accuracy of our method by analyzing and measuring several devices. The results of these analysis will be compared with [17] and [22], and also with the commercial software HFSS [29]. This is to test the accuracy of the method and to compare the computation times for each analysis tool.

The first two designs (Figs. 7 - 10) first appeared in [17] and here we compare the results provided by with our method with those presented in [17].

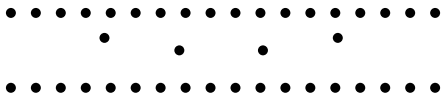

Fig. 7: Three cavity filter (28GHz) [17]

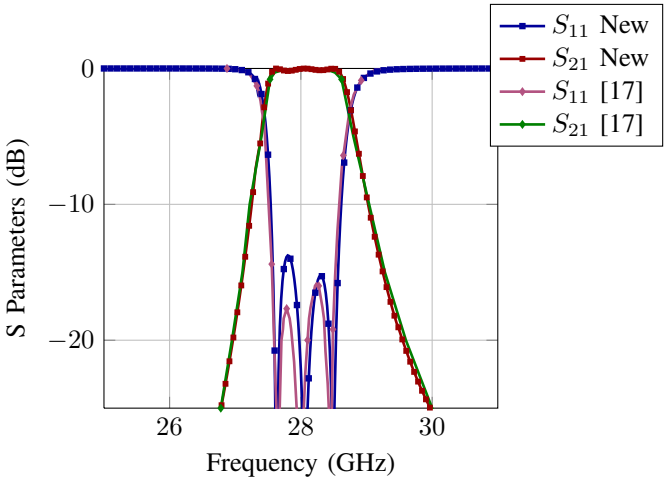

Fig. 8: S Parameters of the circuit in Fig.7

	Total Time
New Method	6.8183 s
[17]	2 min
HFSS	11 min

Table I: Cost comparison for filter in Fig. 7 (60 frequency points)

Table I shows how this method reduces the computational time by 98.96% comparing it with HFSS temporal costs, but it is also in the order of 20 times faster than the hybrid analysis method for SIW structures presented

in [17]. It must be said that the comparisons with HFSS have been done with respect to the discrete sweep, to fairly contrast the results because, although HFSS has also a fast sweep it does not analyze the problem in all the frequencies and the results are less accurate and limited to a certain bandwidth.

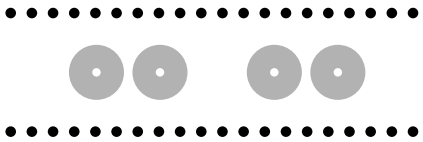

Fig. 9: Dual-band filter with annular dielectric posts [17]

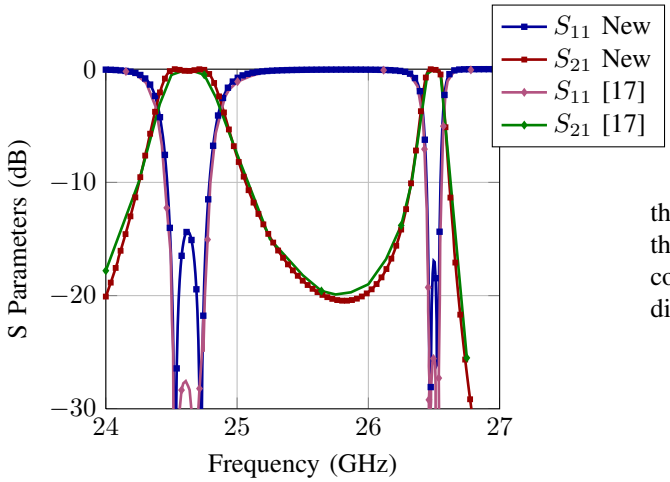

Fig. 10: S Parameters of the circuit in Fig. 9

The fourth design (Figs. 11 - 13), which we already presented in [22], is here analyzed with the new method and compared with [22] and also with the results obtained from the analysis with HFSS.

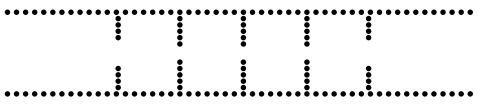

Fig. 11: Four cavity filter (11GHz)

	Time/point	Total Time
New Method	1.4091 s	11.7659 min
[22]	2.3243 s	19.4081 min
HFSS	2.25 min	18.79 hrs

Table II: Cost comparison for filter in Fig. 11 (501 frequency points)

Once again Table II shows that the new method reduces by 98.96% the computational time compared to HFSS discrete sweep, and still using the fast sweep in HFSS

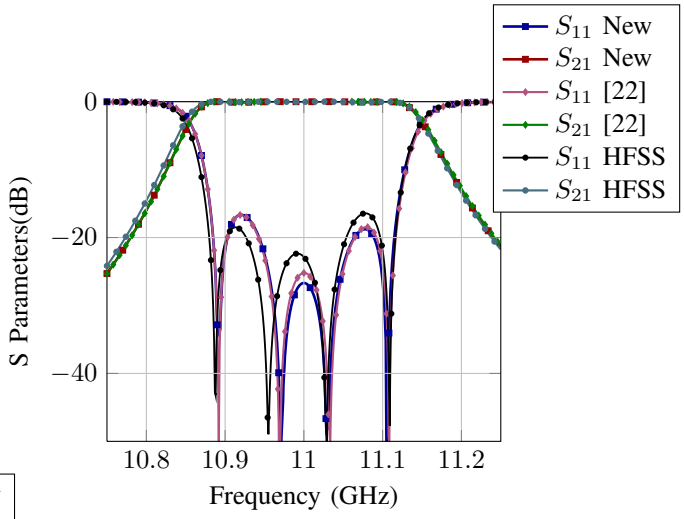

Fig. 12: S Parameters for filter in Fig. 11

the temporal cost would be 20min, twice the cost of the new method's cost. But here we can also see that it considerably reduces the time with respect to [22] using discrete sweep.

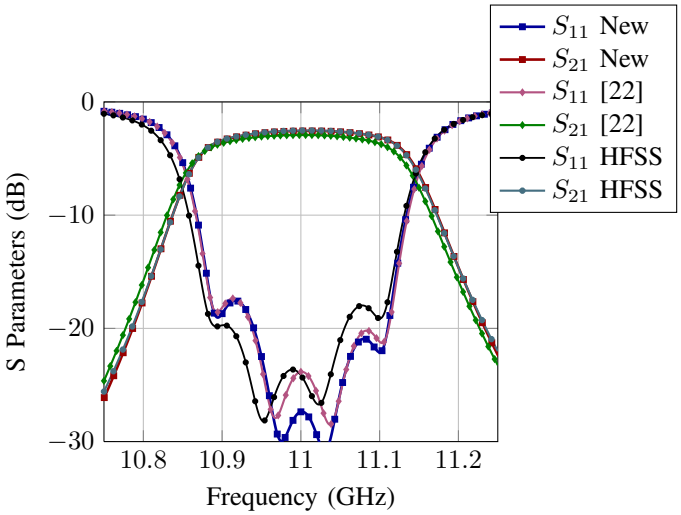

Fig. 13: S Parameters of the filter in Fig. 11 with substrate of $\tan\delta = 0.0023$ and $\sigma = 5.813 \cdot 10^7$ S/m for the metallic posts

	Time/point	Total Time
New Method	1.4295 s	11.9365 min
[22]	5.4615 s	45.6030 min
HFSS	2.25 min	18.79 hrs

Table III: Cost comparison for filter in Fig. 11 with losses (501 frequency points)

As it can be appreciated in Table III, this new method does not increase the computational cost of the analysis because of the fact of introducing losses in the analysis.

The fifth and last design (Figs. 14- 15), first appeared in [17], was already analyzed, redesigned, fabricated, and measured in [22], and now we analyze it again with the new method presented in this work.

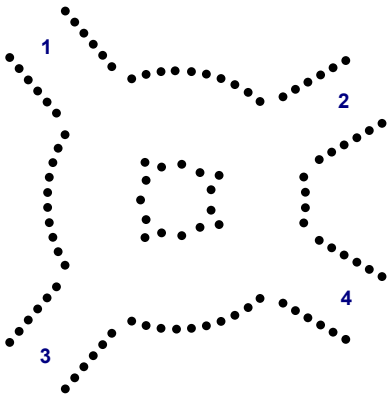

Fig. 14: Hybrid ring

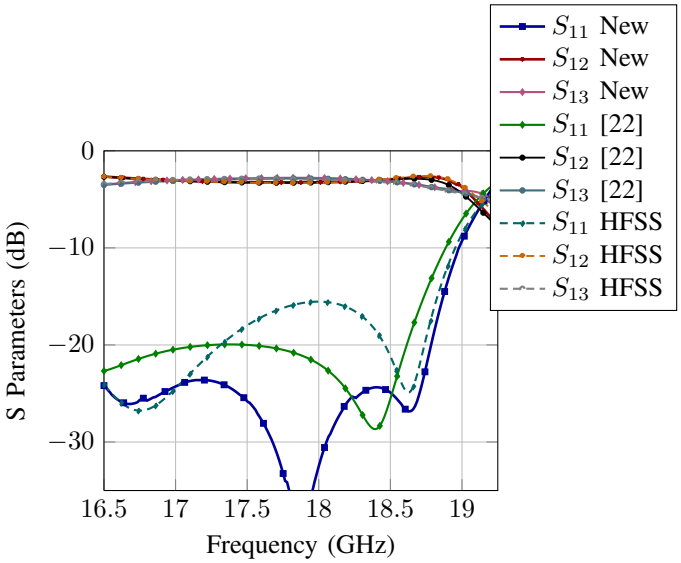

Fig. 15: S Parameters of the circuit in Fig. 14

IV. CONCLUSIONS

We have obtained a very accurate method to efficiently analyze different kinds of SIW devices with multiple accessing ports with an important time saving when compared to other existing methods or to reference commercial software.

It is an extension of the mode matching in [24], where the use of a circular boundary for the mode matching allows the solution of the required integrals by using the fast Fourier transform where analytic solution is not possible, although here the SIW device is not completely surrounded with accessing ports, contrary to [24]. The efficiency of this technique has been tested with the analysis of different topologies, and it is maximum for any kind of circular obstacles such as the studied ones. However, and although these are the most common objects presented in a SIW structure, the method is valid for general arbitrarily shaped posts once we know their scattering matrix.

Furthermore, the new method easily models the losses due to the substrate and the finite conductivity of the metallic posts by taking substrate $\tan\delta$ into account in the calculation of permittivity and phase constant and characterizing the metallic post with the scattering matrix of a dielectric post with their respective permittivities. This way of dealing with losses does not increase the computational cost of the analysis as happens with other methods.

REFERENCES

[1] E. Mehrshahi, M. Salehi, and R. Rezaiesarlak, "Substrate integrated waveguide filters with stopband performance improvement," in *International Conference on Microwave and Millimeter Wave Technology (ICMMT)*. IEEE, 2010, pp. 2018–2020.

[2] B. Chen, T. Shen, and R. Wu, "Dual-band vertically stacked laminated waveguide filter design in LTCC technology," *IEEE Transactions on Microwave Theory and Techniques*, vol. 57, no. 6, pp. 1554–1562, 2009.

[3] H. Chien, T. Shen, T. Huang, W. Wang, and R. Wu, "Miniaturized bandpass filters with double-folded substrate integrated waveguide resonators in LTCC," *IEEE Transactions on Microwave Theory and Techniques*, vol. 57, no. 7, pp. 1774–1782, 2009.

[4] F. Xu and K. Wu, "Guided-wave and leakage characteristics of substrate integrated waveguide," *IEEE Trans. Microwave Theory Tech.*, vol. 53, no. 1, pp. 66–72, Jan. 2005.

[5] J. Hirokawa and M. Ando, "Single-layer feed waveguide consisting of posts for plane TEM wave excitation in parallel plates," *IEEE Trans. on Antennas and Propagation*, vol. 46, no. 5, pp. 625 –630, May 1998.

[6] D. Deslandes and K. Wu, "Accurate modeling, wave mechanisms, and design considerations of a substrate integrated waveguide," *IEEE Trans. on Microwave Theory and Techniques*, vol. 54, no. 6, pp. 2516 –2526, Jun. 2006.

[7] M. Bozzi, L. Perregrini, and K. Wu, "Direct Determination of Multi-mode Equivalent Circuit Models for Discontinuities in Substrate Integrated Waveguide Technology," in *Microwave Symposium Digest, 2006. IEEE MTT-S International*. IEEE, 2007, pp. 68–71.

[8] ——, "Modeling of losses in substrate integrated waveguide by boundary integral-resonant mode expansion method," in *Microwave Symposium Digest, IEEE MTT-S International*. IEEE, 2008, pp. 515–518.

[9] F. Mira, A. San Blas, V. Boria, and B. Gimeno, "Fast and accurate analysis and design of substrate integrated waveguide (SIW) filters," in *Microwave Conference, 2007. European*. IEEE, 2007, pp. 170–173.

[10] F. Mira, A. San Blas, S. Cogollos, V. Boria, and B. Gimeno, "Computer-aided design of substrate integrated waveguide filters for microwave and millimeter-wave applications," in *Microwave Conference, 2009. EuMC 2009. European*. IEEE, 2009, pp. 425–428.

[11] F. Xu, Y. Zhang, W. Hong, K. Wu, and T. Cui, "Finite-difference frequency-domain algorithm for modeling guided-wave properties of substrate integrated waveguide," *IEEE Transactions on Microwave Theory and Techniques*, vol. 51, no. 11, pp. 2221–2227, 2003.

[12] F. Xu, K. Wu, and W. Hong, "Domain decomposition FDTD algo-

rithm combined with numerical TL calibration technique and its application in parameter extraction of substrate integrated circuits," *IEEE Transactions on Microwave Theory and Techniques*, vol. 54, no. 1, pp. 329–338, 2006.

[13] E. Arnieri and G. Amendola, "Analysis of Substrate Integrated Waveguide Structures Based on the Parallel-Plate Waveguide Green's Function," *IEEE Transactions on Microwave Theory and Techniques*, vol. 56, no. 7, pp. 1615–1623, 2008.

[14] E. Abaei, E. Mehrshahi, and H. Sadreazami, "Analysis of substrate integrated waveguide based on two dimensional multiport method," in *International Conference on Microwave and Millimeter Wave Technology (ICMMT)*. IEEE, 2010, pp. 793–796.

[15] R. Rezaiesarlak, E. Mehrshahi, and H. R. Sadreazami, "Hybrid of moment method and mode matching technique to study substrate integrated waveguide," in *International Conference on Microwave and Millimeter Wave Technology (ICMMT)*, 2010, pp. 1980–1982.

[16] C. Balanis, *Advanced Engineering Electromagnetics*. John Wiley & Sons, 1989.

[17] X. Wu and A. Kishk, "Hybrid of method of moments and cylindrical eigenfunction expansion to study substrate integrated waveguide circuits," *IEEE Trans. on Microwave Theory and Techniques*, vol. 56, no. 10, pp. 2270 –2276, Oct. 2008.

[18] ——, "A Hybrid Method to Study the Substrate Integrated Waveguide Circuit," in *Microwave Conference. APMC 2007. Asia-Pacific*. IEEE, 2007, pp. 1–4.

[19] D. Deslandes and K. Wu, "Integrated microstrip and rectangular waveguide in planar form," *IEEE Microwave and Wireless Components Letters*, vol. 11, no. 2, pp. 68–70, Feb. 2001.

[20] ——, "Single-substrate integration technique of planar circuits and waveguide filters," *IEEE Trans. on Microwave Theory and Techniques*, vol. 51, no. 2, pp. 593–596, 2003.

[21] A. Belenger, H. Esteban, V. E. Boria, C.Bachiller, and J. V. Morro, "Hybrid mode matching and method of moments method for the full-wave analysis of arbitrarily shaped structures fed through canonical waveguides using only electric currents," *IEEE Trans. Microwave Theory Tech.*, vol. 58, no. 3, pp. 537–544, March 2010.

[22] A. Belenguer, H. Esteban, E. Diaz, C. Bachiller, J. Cascon, and V. E. Boria, "Hybrid technique plus fast frequency sweep for the efficient and accurate analysis of substrate integrated waveguide devices," *IEEE Trans. on Microwave Theory and Techniques*, vol. 59, no. 3, pp. 552 –560, March 2011.

[23] H. Esteban, S. Cogollos, V. Boria, A. Blas, and M. Ferrando, "A new hybrid mode-matching/numerical method for the analysis of arbitrarily shaped inductive obstacles and discontinuities in rectangular waveguides," *IEEE Trans. on Microwave Theory and Techniques*, vol. 50, no. 4, pp. 1219 –1224, Apr. 2002.

[24] C. Bachiller, H. Esteban, H. Mata, M. Valdes, V. Boria, A. Belenguer, and J. Morro, "Hybrid mode matching method for the efficient analysis of metal and dielectric rods in H-plane rectangular waveguide devices," *IEEE Trans. on Microwave Theory and Techniques*, vol. 58, no. 12, pp. 3634 –3644, Dec. 2010.

[25] H. Esteban, S. Cogollos, C. Bachiller, A. S. Blas, and V. E. Boria, "A new analytical method for the analysis of multiple scattering problems using spectral techniques," in *IEEE Antennas and Propagat. Society Int. Symp.*, San Antonio Texas, Junio 2002, pp. 82–85.

[26] M. Baquero, "Transformaciones espectrales y aplicaciones a síntesis de ondas, medida de antenas y difracción," Ph.D. dissertation, Universitat Politècnica de València, València, 1994.

[27] M. O. Kolawole, "Scattering from dielectric cilinders having radially layered permitivity," *J. of Electromagnetic Waves and Applications*, vol. 6, no. 2, pp. 235–239, 1992.

[28] Z. Hao, W. Hong, J. Chen, X. Chen, and K. Wu, "Planar diplexer for microwave integrated circuits," *IEEE Proc. on Microwave Antennas and Propagat.*, vol. 152, no. 6, pp. 455–459, Dec. 2005.

[29] Ansoft Corporation, "HFSS: 3D high-frequency electromagnetic simulation." [Online]. Available: http://www.ansoft.com/products/hf/hfss/index.cfm

Elena Díaz Caballero (S'07-GSM'10) received the Telecommunication Engineering degree from the Universidad Politécnica de Valencia (UPV), Spain, in July 2010. She is now working on her research toward the Ph.D. degree at UPV, where she was awarded Student of the Year in 2010. She won a Collaboration Fellowship at the Communications Department of UPV in 2009, has done an internship at AURORASAT Company and has recently won an Excellence Fellowship from the UPV. Her research interest is currently focused in the development of efficient methods for the analysis and design of substrate integrated waveguide devices.

Héctor Esteban (S'93−M'99) received a degree in telecommunications engineering from the Universidad Politécnica de Valencia (UPV), Spain, in 1996, and a Ph.D. degree in 2002. He worked with the Joint Research Centre, European Commission, Ispra, Italy. In 1997, he was with the European Topic Centre on Soil (European Environment Agency). He rejoined the UPV in 1998. His research interests include methods for the full- wave analysis of open-space and guided multiple scattering problems, CAD design of microwave devices, electromagnetic characterization of dielectric and magnetic bodies, and the acceleration of electromagnetic analysis methods using the wavelets and the FMM.

Angel Belenguer (M'04) received the Telecommunication Engineering and Ph.D. degrees from the Universidad Politécnica de Valencia, Spain, in 2000 and 2009, respectively. He joined the Universidad de Castilla-La Mancha in 2000, where he is now Profesor Titular de Escuela Universitaria in the Departamento de Ingeniería Eléctrica, Electrónica, Automática y Comunicaciones. His research interests include methods in the frequency domain for the full-wave analysis of open-space and guided multiple scattering problems, specifically the improvement or acceleration of these methods using several strategies: hybridization of two or more different methods, the use of specific basis, and the application of accelerated solvers or solving strategies to new problems or structures.

Vicente E. Boria (S'91−A'99−SM'02) received the *Ingeniero de Telecomunicacin* and the *Doctor Ingeniero de Telecomunicacin* degrees from the Universidad Politécnica de Valencia, Spain, in 1993 and 1997. In 1993 he joined the Universidad Politécnica de Valencia where he is Full Professor since 2003. In 1995 and 1996 he was held a Spanish Trainee position with the European Space research and Technology Centre (ESTEC)-European Space Agency (ESA). He has served on the Editorial Boards of the IEEE Transactions on Microwave Theory and Techniques. His current research interests include numerical methods for the analysis of waveguide and scattering structures, automated design of waveguide components, radiating systems, measurement techniques, and power effects in passive waveguide systems.